



# Cytotoxicity of aptamer-conjugated chitosan encapsulated mycogenic gold nanoparticles in human lung cancer cells

Xiaowen Hu<sup>1</sup> · Kandasamy Saravanakumar<sup>1</sup> · Anbazhagan Sathiyaseelan<sup>1</sup> · Vinothkumar Rajamanickam<sup>2</sup> · Myeong-Hyeon Wang<sup>1</sup>

Received: 29 April 2021 / Accepted: 3 August 2021 / Published online: 4 October 2021  
© Islamic Azad University 2021

## Abstract

The present work investigated the cytotoxicity of aptamer (Apt)-conjugated chitosan (CST) encapsulated mycogenic (*Talaromyces purpureogenus* (Tp)) gold nanoparticles (AuNPs) in human lung cancer cell line. A total of three steps were involved in the fabrication of Apt-CST-Tp-AuNPs: (i) mycogenic synthesis of Tp-AuNPs using mycelial extract of *T. purpureogenus*, (ii) encapsulation of the chitosan on Tp-AuNPs (CST-Tp-AuNPs), and (iii) conjugation of Apt in CST-Tp-AuNPs to form final material of Apt-CST-Tp-AuNPs. The nanoparticles Tp-AuNPs and Apt-CST-Tp-AuNPs were found to be hexagonal shaped with the size of  $37.06 \pm 6.70$  nm and  $62.05 \pm 15.22$  nm, respectively, observed by TEM analysis. But the DLS analysis showed the hydrodynamic size of Apt-CST-Tp-AuNPs was  $91.67 \pm 2.15$  nm with a zeta potential of  $47.31 \pm 0.63$  mV while Tp-AuNPs exhibited the hydrodynamic size of  $56.13 \pm 1.65$  nm with a zeta potential of  $-58.83 \pm 1.64$  mV. The size differences in the TEM and DLS analysis are attributed to the hydrodynamic nature of nanoparticles. The FTIR analysis demonstrated the capping of the mycelial extract on the surface of Tp-AuNPs and Apt-CST-Tp-AuNPs. The Apt-CST-Tp-AuNPs did not show cytotoxicity to human embryonic kidney cells (HEK293) while it showed ~60% of cell death in human lung cancer cells (A549). The annexin V FITC and PI staining results revealed that Apt-CST-Tp-AuNPs induced higher cell death (~8.60%) in A549 cells than Tp-AuNPs and CST-Tp-AuNPs. The Apt-CST-Tp-AuNPs triggered cytotoxicity in A549 cells through M1 phase cell cycle arrest and regulating the apoptosis-related protein (Bcl-2 and Bax) expressions. These results demonstrated the effective cytotoxic activity of Apt-CST-Tp-AuNPs in A549 cells.

---

Xiaowen Hu and Kandasamy Saravanakumar have equally contributed.

---

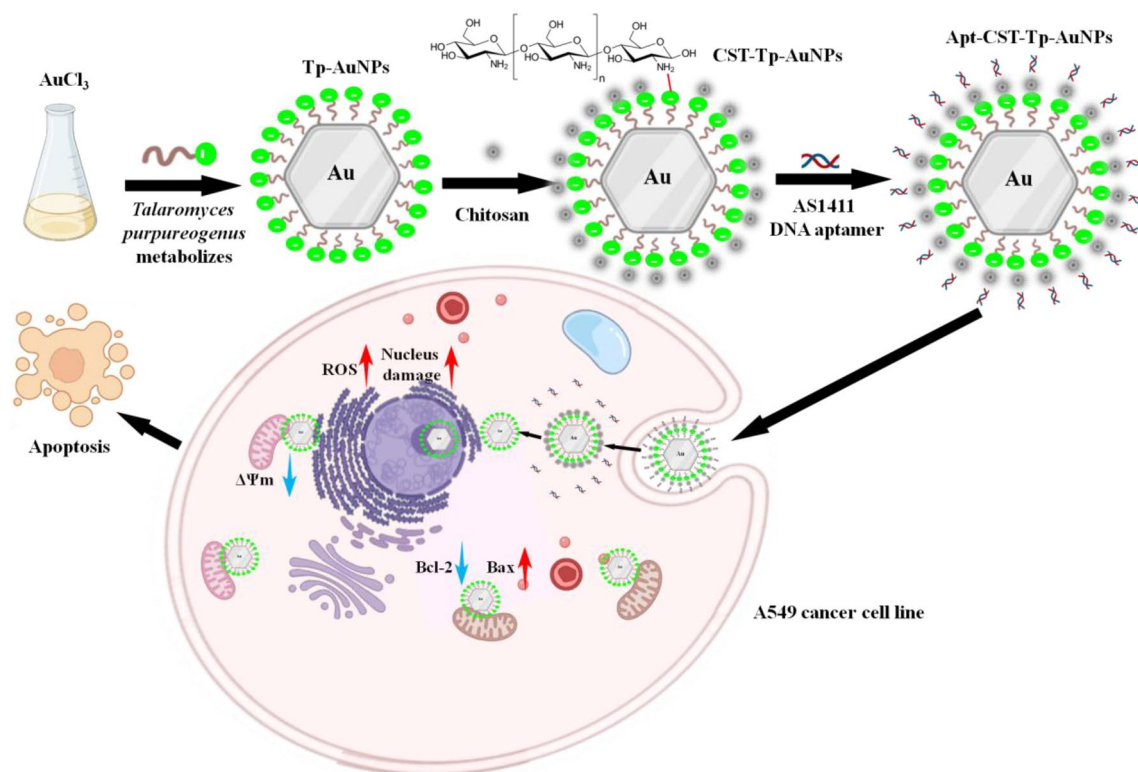
✉ Myeong-Hyeon Wang  
mhwang@kangwon.ac.kr

<sup>1</sup> Department of Bio-Health Convergence, Kangwon National University, Chuncheon 200-701, South Korea

<sup>2</sup> Key Laboratory of Imaging Diagnosis and Minimally Invasive Intervention Research, School of Medicine, Lishui Central Hospital, Lishui Hospital of Zhejiang University, The Fifth Affiliated Hospital of Wenzhou Medical University, Lishui 323000, China



## Graphic abstract



**Keywords** Aptamer · Endophytic fungi · Gold nanoparticles · Chitosan · Human lung cancer

## Introduction

Lung cancer is the second leading cancer that occurred in both men and women. According to the cancer statistics 2019, new cancer patients have been reported ~ 1,762,450 in the United States, of which ~ 13% belong to lung cancer. Cancer-related death is reported about 606,880 in the USA, in which ~ 24% death is caused by lung cancer [1]. The early diagnosis of cancer can reduce the risk of metastases that results in less mortality and morbidity. Therefore, the early diagnosis and targeted cancer therapy methods are received more attention over conventional therapeutics such as chemotherapy, surgery, and radiotherapy [2]. In this context, aptamer-functionalized drug delivery system gained importance in cancer therapeutics because of its ability to specifically bind to overexpressed cancer cell surface nucleolin which is highly expressed in cancer cells. Among the aptamer, AS1411 consists of 26-mer oligonucleotides with unique G-rich quadruplex structures that have been used as a promising ligand to target the overexpressed nucleolin in tumors [3, 4].

Gold nanoparticles (AuNPs) have been used in versatile applications such as medicine, chemistry, biology, physics, and material science [5]. Especially in nanomedicine, AuNPs have been used as a potential drug carrier or photothermal agent due to their inert nature and less toxicity to normal cells [6–8]. The green synthesis of the AuNPs is economically feasible and ecology suitable but the physical and chemical methods are stand with several limitations including extreme synthesis conditions, toxic or harsh chemicals release, and laborious [9]. Moreover, recent studies from our group have reported that the green synthesis AuNPs is acted as a base material for the preparation of a pH-responsive drug carrier system to deliver drugs in cancer sites through nucleolin targeting mechanism [10–12].

The endophytic fungi are known to inhabit in internal tissues of the plant without causing any damage to the host [13]. The mycogenic NPs synthesized from the endophytic fungi are promising in antioxidant, antibacterial, and anticancer activities [14–17]. Among the endophytic fungi, *T. purpureogenus* is isolated from the marine plants or traditional plants pose the higher ability to produce the



novel metabolites (pigment, urea, phenol, propanoic acid, and butanamide) and nanoparticles (silver nanoparticles) with antiproliferative, antioxidative, antibacterial and anticancer properties [18–22]. Chitosan is being used in the development of drug delivery systems because of its non-toxicity, biocompatible properties [23–26]. Moreover, the encapsulation of chitosan with metal nanoparticles enables successful blood circulation and cellular penetration with good stability to targeting the cancer cells based on the pH sensitivity [27, 28]. Moreover, there is no work reported for the myco-synthesis of gold nanoparticles using *T. purpureogenus*. Therefore, this work aimed to synthesis the Tp-AuNPs using the mycelial extract of *T. purpureogenus* and encapsulated with chitosan (CST-Tp-AuNPs), further conjugated by aptamer (Apt-CST-Tp-AuNPs) (Scheme 1) for improved cytotoxicity in the human lung cancer cells.

## Materials and methods

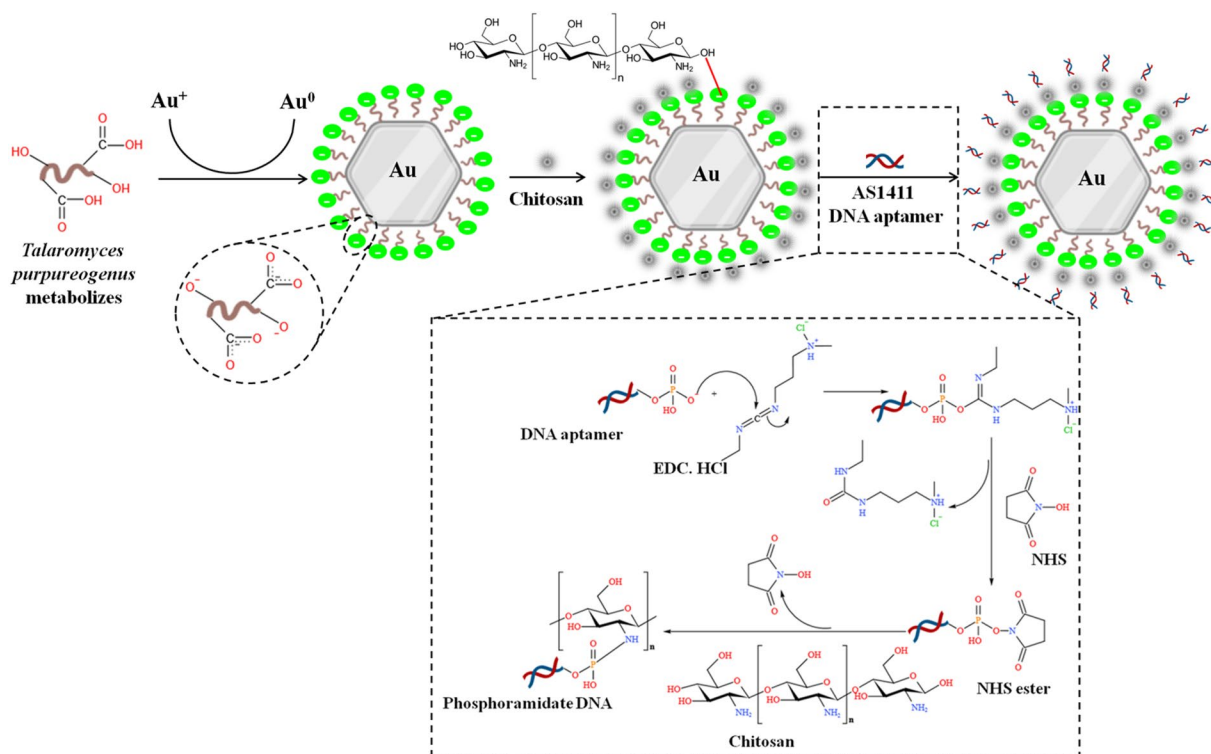
### Materials

Endophytic fungal strain *T. purpureogenus* (NCBI GenBank accession number: MK108915) was previously isolated from the leaves of *Pinus densiflora* S. et Z. were used in the present study. Gold (I) chloride (AuCl), low molecular

weight chitosan (75–85% deacetylated chitin, poly(D-glucosamine), CAS no. 9012-76-4, MW 50,000–190,000 Da based-on viscosity), sodium triphosphate pentabasic (TPP), cell viability assay kit (WST-8 CELLMAX™, MediFab), dichlorofluorescein diacetate (DCFH-DA), propidium iodide (PI), rhodamine 123 (Rh123), ethidium bromide (EB), acridine orange (AO), N-hydroxy succinimide (NHS) and carbodiimide hydrochloride (EDC. HCl) were purchased from Sigma-Aldrich, Republic of Korea. DNA aptamer (AS1411) was procured from Cosmo Genetech, Republic of Korea. The human lung carcinoma (A549) cell line and the human embryonic kidney (HEK293) cell line were obtained from the Korean Cell Line Bank (KCLB, Seoul, Republic of Korea). Dialysis membrane (SnakeSkin™, 10 kDa) and all other staining kits and cell culture medium were obtained from Thermo Fishers Scientific Seoul, Republic of Korea.

### Biosynthesis of Tp-AuNPs using mycelial extract of *T. purpureogenus*

Mycelial extracts of *T. purpureogenus* were prepared according to the standard methods reported earlier [29]. In brief, 2 mL of fungal spore suspension ( $8 \times 10^6$  spores/mL) was inoculated in 200 mL of fresh potato dextrose broth (PDB) in 500-mL Erlenmeyer flasks incubated in shaking incubator at 180 rpm at  $27 \pm 2$  °C for 7 days. The mycelial extract was



**Scheme 1** The mechanisms of Apt-CST-Tp-AuNP preparation



collected by filtration using the Whatman No.1 filter paper. Afterward, 20 mL of mycelial extract were added into 80 mL of AuCl (10 mM) solution and kept in the shaking incubator at 180 rpm at 28 °C in dark conditions for 72 h. The color change from yellow to pink then dark purple was an indication of TP-AuNPs formation and it was recorded using the UV–visible spectrum at different time intervals. Finally, the TP-AuNPs were collected by centrifuge at 17,000 rpm and lyophilized as a powder for further works.

### Encapsulation of chitosan on Tp-AuNPs

The Tp-AuNPs were encapsulated in chitosan according to the method reported previously with minor modifications [30]. In brief, 75 mg of chitosan was dissolved 25 mL of 0.5% acetic acid (aqueous solution, pH  $4.6 \pm 0.1$ ) kept on the magnetic stirrer at 90 rpm at room temperature (RT) overnight. The next day, 5 mg of Tp-AuNPs were added into chitosan solution and again stirred for 30 min at 90 rpm and then sonicated for 10 min. For the fabrication of CST-Tp-AuNPs, 20 mL of sodium triphosphate pentabasic (1.0 mg/mL, aqueous solution) was slowly added into Tp-AuNPs-chitosan solution and kept on the magnetic stirrer at 90 rpm overnight at RT in dark conditions. Finally, the CST-Tp-AuNPs were collected by centrifugation at 17,000 rpm for 15 min.

### Conjugation of aptamer on CST-Tp-AuNPs

The DNA aptamer was conjugated with CST-Tp-AuNPs through covalent bonding activated in CST-Tp-AuNPs through EDC and NHS reaction. In brief, 20  $\mu$ L of EDC (0.1 mg/mL, PBS solution) and 10  $\mu$ L of NHS (0.1 mg/mL, PBS solution) added to 1 mL of CST-Tp-AuNPs (1 mg/mL, aqueous solution) and allowed in 4 °C for 2 h. Then 30  $\mu$ L of aptamer solution were added in CST-Tp-AuNPs and incubated overnight at 4 °C. Afterward, Apt-CST-Tp-AuNPs were dialyzed against deionized water for 12 h at 4 °C using a dialysis membrane (SnakeSkin™, 10 kDa). Finally, the Apt-CST-Tp-AuNPs were collated by lyophilization for further experiments. Besides, the aptamer conjugation with CST-Tp-AuNPs was confirmed by agarose gel electrophoresis [31].

### Characterization of Apt-CST-Tp-AuNPs

The nanoparticles (Tp-AuNPs, CST-AuNPs, and Apt-CST-Tp-AuNPs) were characterized using the field emission transmission electron microscopy (FE-TEM) energy-dispersive X-ray spectroscopy (EDS) (JEM-2100F; Jeol, Tokyo, Japan), Particle Analyzer (Malvern, British), X-ray diffraction (XRD) (X'pert-pro MPD-PANalytical Netherland) and

Fourier transform infrared spectroscopy (FT-IR) (Frontier; PerkinElmer, Waltham, MA, USA).

### In vitro release

The in vitro release of Tp-AuNPs from Apt-CST-Tp-AuNPs was determined by the dialysis membrane diffusion method [31]. In brief, the phosphate buffer (pH 7.4) and acetate buffer (pH 5.4) were used as different pH solutions for pH-responsive nanoparticle release studies. 1 mg/mL of Apt-CST-Tp-AuNPs has been dissolved in the different pH (7.4 and 5.4) buffer solution and transferred to the dialysis bag (12 kDa). Afterward, the dialysis bag was incubated in 50 mL of dissolution buffer (pH 7.4 and 5.4) at 37 °C under mild stirring (50 rpm). Followed by 5 mL of aliquot were collected from dissolution buffer at a different time interval to measure the release of nanoparticles in terms of absorbance by UV spectrophotometer.

### Cell culture

The human lung cancer cell line (A549) and the human embryonic kidney cell line (HEK293) were cultured in RPMI-1640 and DMEM medium, respectively, at 37 °C in a 5% CO<sub>2</sub> humidified incubator. These culture mediums were previously incorporated with 10% fetal bovine serum (FBS) and 1% penicillin and streptomycin (PS).

### Cytotoxicity

Cytotoxicity of nanoparticles was determined by the WST assay [12]. 100  $\mu$ L/well of A549 or HEK293 cells ( $1 \times 10^4$ ) was seeded in a 96-well plate and incubated in a CO<sub>2</sub> (5%) incubator at 37 °C for 24 h. After reaching 80–90% confluence, the different concentrations (1.9–1000  $\mu$ g/mL) of nanoparticles or mycelial extract were treated for 24 h. After the treatment, the cell death was measured by adding the WST reagent (10  $\mu$ L/well) and incubated in the above-mentioned condition for 1 h. After the incubation period, the optical density was measured at 450 nm using a 96-well plate reader (SpectraMax® Plus Microplate Reader from Molecular Devices). The percentage of cytotoxicity was measured according to the formula described earlier [32].

### Fluorescent staining analysis

The fluorescent stain dichloro-dihydro-fluorescein diacetate (DCFH-DA) was used for the measurement of reactive oxygen species (ROS) generation. Propidium iodide (PI) stain was used to observe the nucleus damage while mitochondrial membrane potential loss ( $\Delta\psi_m$ ) was studied using stain rhodamine 123 (Rh123). The NPs-induced apoptosis stages were visualized using the dual stain acridine

orange (AO)/ethidium bromide (EB). In brief, the A549 cells ( $1 \times 10^4$ ) were seeded in a 12-well plate and incubated in a 5% CO<sub>2</sub> incubator at 37 °C for 24 h. After 24 h, the 50 μL of IC<sub>50</sub> concentration of different samples were treated for 24 h. Finally, the different samples induced ROS generation, nucleus damage, Δψ<sub>m</sub> loss were observed using the above-mentioned stains by fluorescent microscopy (Olympus CKX53, Tokyo, Japan).

### Flow cytometry analysis

**Detection of cell death by annexin V FITC and PI staining** The human lung cancer (A549) cells were cultured in the T-25 flask containing the RPMI and allowed in the 5% CO<sub>2</sub> incubator to reach 80–90% of cell confluence. Then the cells were treated with IC<sub>50</sub> concentrations of different samples (Tp, Tp-AuNPs, CST-Tp-AuNPs, and Apt-CST-Tp-AuNPs) for 6 h. After the treatments, the cells were collected by scrapping method and centrifuged at 2000 rpm for 3 min. Then the cells were washed twice with cold PBS followed by centrifuging at 2000 rpm for 3 min. Afterward, the cells were resuspended in 100 μL of 1X annexin binding buffer then added 5 μL of annexin V-FITC (1 mg/mL) and 1 μL of PI (100 μg/mL) and incubated for 15 min at RT. Finally, the stained cell suspension made up to 500 μL using the 1X annexin binding buffer, then immediately analyzed by FACS caliber (BD FACScaliber, BD, California, USA).

**Cell cycle** For the cell cycle assay, the cell preparation and treatments were done as described in “[Detection of cell death by annexin V FITC and PI staining](#)”. But in this experiment, the 0.5 mL of PI stock (50 μg/mL of PI and 100 μg/mL RNase A in PBS) was used as the staining solution and incubated for 30 min at RT and then analyzed by FACS caliber (BD FACScaliber, BD, California, USA).

### Western blotting

The effect of the different nanoparticles on the expression of the apoptosis-related protein was detected by western blotting [33]. In brief, the protein was extracted by lyse cells in RIPA buffer (150 mM NaCl, 1% NP-40, 0.5% NaDC, 0.1% SDS, 50 mM Tris pH 8.0, 25 mg/mL aprotinin and 50 mg/mL leupeptin). Protein concentration was measured by Bradford assay. Followed by this, protein (20–30 μg) was separated using 10% SDS-PAGE and transferred to the membrane for 2 h at 70 V. Subsequently, the membrane was incubated in blocking buffer BSA (Cohn fraction V) solution for 1 h in RT. The specific primary antibodies B-cell lymphoma 2 (Bcl-2), Bcl-2-associated X protein (Bax), and β-actin were used against a protein on the membrane overnight at 4 °C. The membrane was washed by TBST for more than 5 min before application of secondary antibody-labeled

horseradish peroxidase for 2 h in RT. Finally, the intensities of each band were detected by Image-Pro Plus.

## Results and discussion

### Characterization of nanoparticles

#### UV-visible spectrum

UV-visible spectrum analysis is used to determine the synthesis, size, and shape of nanoparticles [34]. In general, the localized surface plasmon resonance (LSPR) of gold nanoparticles (AuNPs) results in a strong absorbance band in the visible region (500–600 nm). The smaller nanospheres (4–25 nm) primarily absorb the light and exhibit peaks near 520 nm, while larger spheres exhibit increased scattering and significantly broad peaks. The larger spheres scatter and more light optical cross sections are exhibited because their albedo (a ratio of scattering to total extinction) increases with size. The change in the shape of the nanoparticle would also cause the difference in the area of the optical cross section, which results in different refractive index and reflectivity, thus affecting the blue shift or red shift of the absorption peak [34]. The mycogenic Tp-AuNPs showed a strong absorbance peak at 540 nm corresponding to the LSPR relation of gold due to color changes from yellow to light pink (Fig. 1A), which illustrated the size of nanoparticles may be larger than 25 nm and the shape of nanoparticles may not exactly sphere. Similar results of UV-Vis spectrum have been reported for AuNPs synthesized various endophytic fungi [35, 36]. Moreover, the absorbance peak of CST-Tp-AuNPs was a little red-shifted compared to Tp-AuNPs (Fig. 1B), which foreboded that the size of CST-Tp-AuNPs was expected to be large than the Tp-AuNPs, or the shape of CST-Tp-AuNPs may be different from Tp-AuNPs. This result was similar to the previous work [10]. Moreover, the size increase might be caused due to methods of chitosan encapsulation, the concentration of TPP, or the absence of TPP [37].

#### DLS and XRD analyses

The size, poly dispersion index (PDI), and ζ-potential of CST-Tp-AuNPs and Tp-AuNPs were determined by DLS (Figs. 2 and 3). The DLS indicated that the size of Tp-AuNPs and CST-Tp-AuNPs was  $56.13 \pm 1.65$  nm and  $91.67 \pm 2.15$  nm, respectively (Fig. 2A, B). The ζ potential is the charge carried on the surface of the particle. According to the repulsion principle, the positively charged electrode attracts the oppositely charged electrode; therefore, the higher ζ potential charge could result in the larger ion surface that assists the dispersion and stability



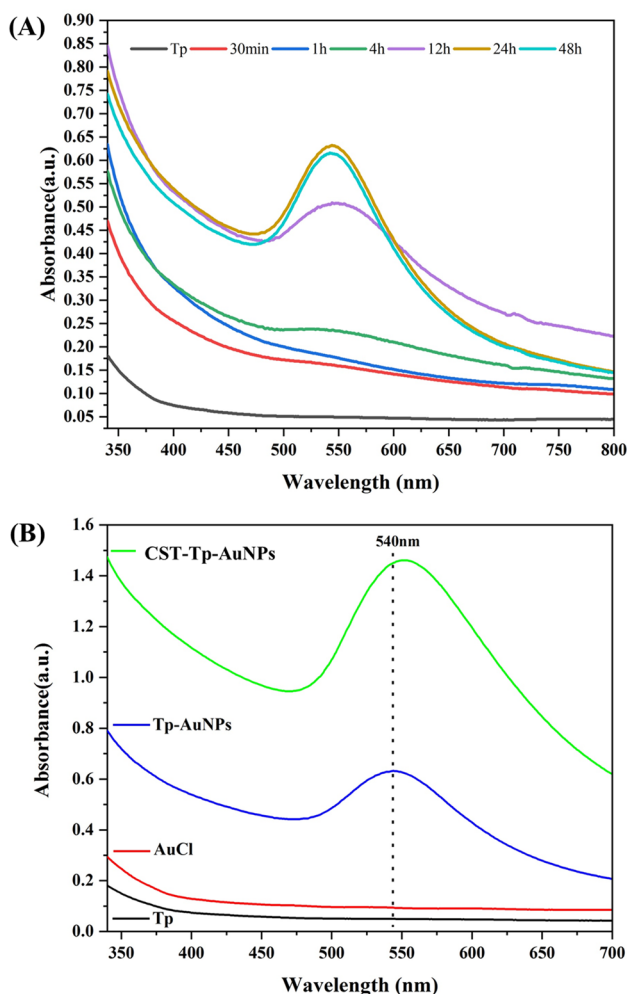


**Fig. 1** UV-visible spectrophotometer analysis. Effect of different time intervals in the synthesis of Tp-AuNPs (A), comparison of UV-visible spectral analysis of CST-Tp-AuNPs, Tp-AuNPs, gold chloride (AuCl) and mycelial extract (Tp) (B)

of the NPs [38, 39]. The Tp-AuNPs showed a  $\zeta$ -potential of  $-58.83 \pm 1.64$  mV while CST-Tp-AuNPs exhibited a  $\zeta$ -potential of  $47.31 \pm 0.63$  mV (Fig. 3A, B). These zeta results indicated that both NPs were highly stable with a negative charge for Tp-AuNPs and positive charge CST-Tp-AuNPs due to capping and encapsulation of fungal metabolites and chitosan, respectively. Moreover, the present results were in agreement with several earlier results that report the green-synthesized gold nanoparticles with negative  $\zeta$ -potential [40–42]. However, the CST-Tp-AuNPs showed a positive charge due to encapsulation of chitosan and its higher positive charge might be the reason for the  $\zeta$ -potential charge CST-Tp-AuNPs [43, 44]. The XRD results of these two nanoparticles were found to be crystalline (Fig. 4A, B). The XRD results showed the characteristic peaks of Tp-AuNPs ascribed to Bragg reflections at (111), (200), and (220) due to  $2\theta$  values of  $31.73^\circ$ ,  $45.44^\circ$ ,

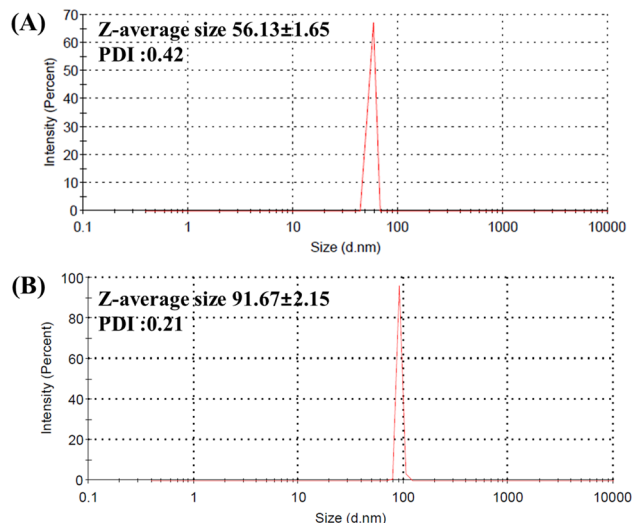


**Fig. 2** Dynamic light scattering (DLS) analysis of mycogenic gold nanoparticles Tp-AuNPs synthesized using the mycelial extract of *Talaromyces purpureogenus* (A) and chitosan encapsulated (CST-Tp-AuNPs) prepared by ionic gelation and covalent bonding method (B)

and  $66.24^\circ$ , respectively (Fig. 4A). Similarly, the CST-Tp-AuNPs exhibited the characteristic peaks ascribed to Bragg reflections at (111), (200), (220), (311), and (222) due to  $2\theta$  values of  $31.72^\circ$ ,  $45.48^\circ$ ,  $56.48^\circ$ ,  $75.27^\circ$  and  $83.98^\circ$ , respectively (Fig. 4B). The Tp-AuNPs showed intense diffraction at  $31.73^\circ$ , while the CST-Tp-AuNPs showed intense diffraction at  $45.48^\circ$ , which illustrated that the Tp-AuNPs' preferred growth orientation of zero-valent gold was fixed in (111) direction, while the CST-Tp-AuNPs preferred in (200) direction [45]. The XRD pattern exhibited the different angle values between the CST-Tp-AuNPs and Tp-AuNPs due to the variation of shape and size of the nanoparticles [46].

### FTIR analysis

The functional groups of Tp, Tp-AuNPs, and CST-Tp-AuNPs were determined by FTIR analysis (Fig. 5A). The Tp extract exhibited the peak at  $3267\text{ cm}^{-1}$  and  $1377\text{ cm}^{-1}$  in relation to the typical stretching vibration of O–H, the peak at  $2923\text{ cm}^{-1}$  and  $1637\text{ cm}^{-1}$  were due to C–H and C=C stretching of alkane and cyclic alkene. These functional vibrations were indicated the presence of phenolic compounds in Tp extract [47]. Meanwhile, the other peaks including  $1546\text{ cm}^{-1}$ ,  $1309\text{ cm}^{-1}$ ,  $1245\text{ cm}^{-1}$ ,  $1150\text{ cm}^{-1}$ , and  $1027\text{ cm}^{-1}$  were ascribed to fungal secondary metabolites such as terpenoids, pigment, and enzyme [48]. The Tp-AuNPs exhibited the peaks at  $2918\text{ cm}^{-1}$ ,  $1450\text{ cm}^{-1}$ , and  $1043\text{ cm}^{-1}$  were corresponding to C–H stretching, and C–N, respectively. Also, Tp-AuNPs have displayed some peaks similar to Tp extract, which evidenced the capping of Tp extracts on the surface of Tp-AuNPs. The CST-Tp-AuNPs



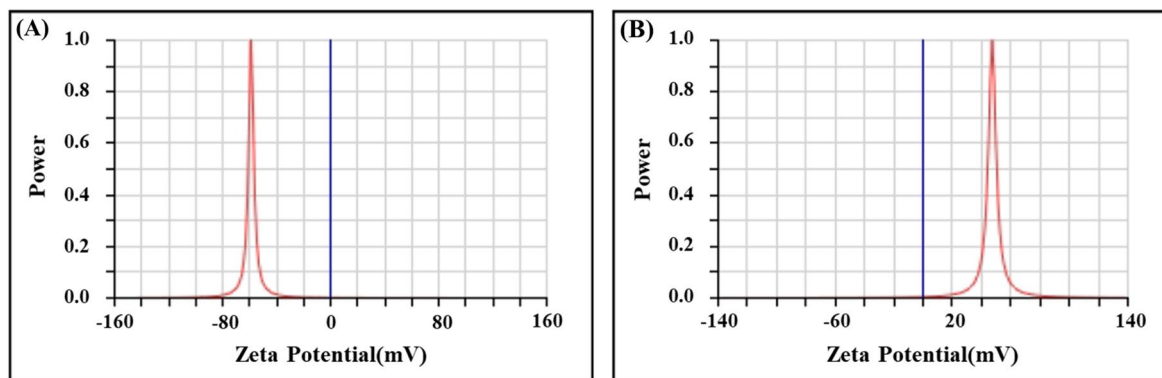


**Fig. 3** Zeta potential analysis of gold nanoparticles (Tp-AuNPs) synthesized by using the mycelial extract of *Talaromyces purpureogenus* (A) chitosan encapsulated CST-Tp-AuNPs (B) by DLS

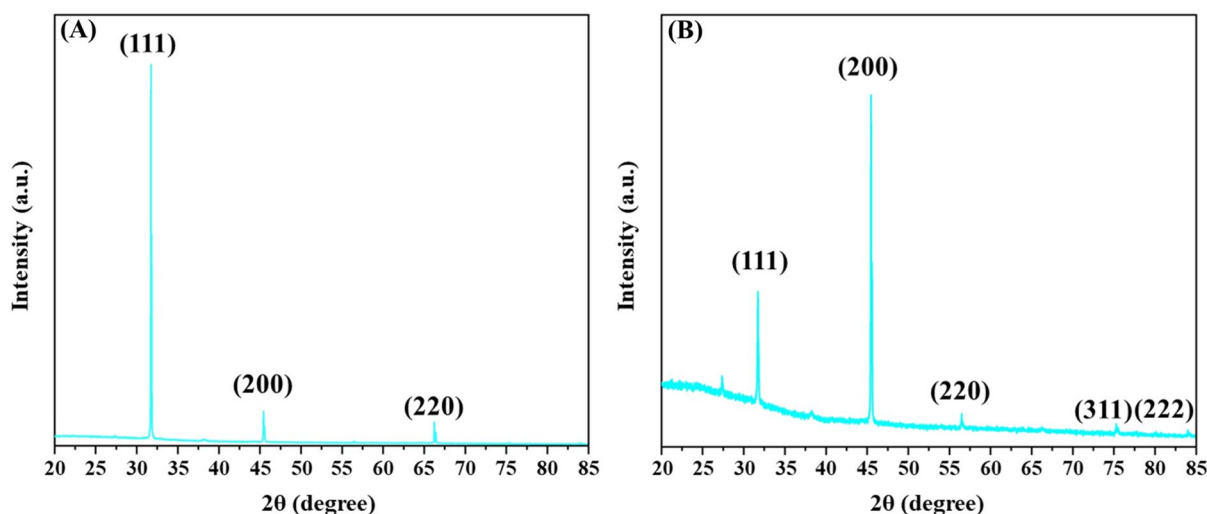


**Fig. 4** X-ray diffraction (XRD) pattern for Tp-AuNPs synthesized by using the mycelial extract of *Talaromyces purpureogenus* (A) CST-Tp-AuNPs prepared by TPP-ionic gelation method (B)

showed the peak at  $1740\text{ cm}^{-1}$ ,  $1630\text{ cm}^{-1}$  which ascribed to C=O and N–H stretching of amide I and amide II as character peaks of chitosan [49]. The aptamer functionalized on CST-Tp-AuNPs did not exhibit any significant peak shifts (data not shown) due to the nitrogenous base-rich aptamer-functionalized surface [50]. Besides, the agarose gel electrophoresis demonstrated the successful conjugation of aptamer in CST-Tp-AuNPs (Fig. 5B). Similarly, earlier work also performed on agarose gel electrophoresis to confirm the conjugation of aptamer in nanoparticles [12].

### TEM and EDS analyses

The size and shape of the nanoparticles are shown in the TEM image (Fig. 6A–C). The size of both nanoparticles was found to be  $< 100\text{ nm}$ . The CST-Tp-AuNPs and the Apt-CST-Tp-AuNPs were a little bigger than Tp-AuNPs

because of chitosan encapsulation. The irregular spheres for Tp-AuNPs and hexagonal crystals for CST-Tp-AuNPs were observed (Fig. 6A, B). The size and shape were found to be different between the nanoparticles due to encapsulation of chitosan, cross-linking of TPP, and pH of nanoparticle suspension [37]. The TEM results were in accordance with UV–visible spectral analysis. Moreover, it observed that the shape and size of Apt-CST-Tp-AuNPs were similar to CST-Tp-AuNPs (Fig. 6C). The proportion of gold in nanoparticles is 57.18%, evidenced by EDS analysis (Fig. 6D, E) in Apt-CST-Tp-AuNPs. Moreover, the size of the particles was found to be smaller in TEM analysis than DLS analysis because the dehydrated particles can only be analyzed under the TEM as DLS is performed in the solution state. Hence, DLS expresses the hydrodynamic size of the particle [10]. Further, the pH-responsive release of the nanoparticle was measured in different pH (SI Fig. 1). The release



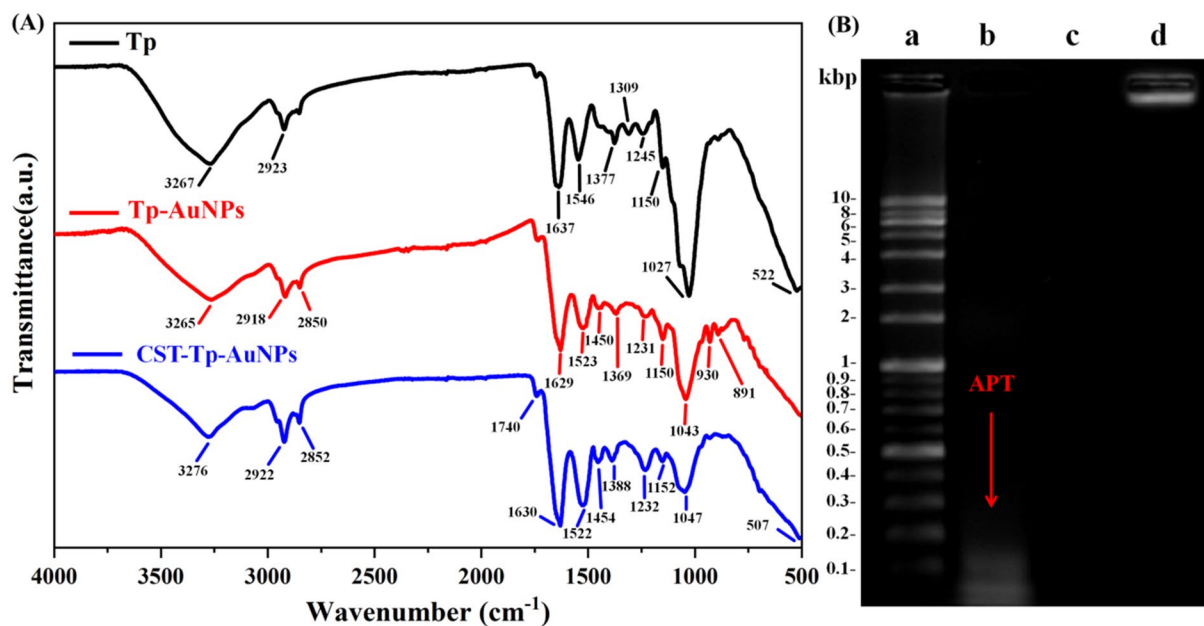


**Fig. 5** Fourier transform infrared spectroscopy (FTIR) analysis of functional group shifting in mycelial extract (Tp), gold nanoparticles (Tp-AuNPs) and chitosan encapsulated gold nanoparticles (CST-Tp-AuNPs) (A). Agarose gel electrophoresis for determination of

aptamer conjugation in nanoparticles (B). In Fig. 4B, the lanes marking is corresponding to DNA Maker (a), aptamer (b), CST-Tp-AuNPs (c) and Apt-CST-Tp-AuNPs (d)

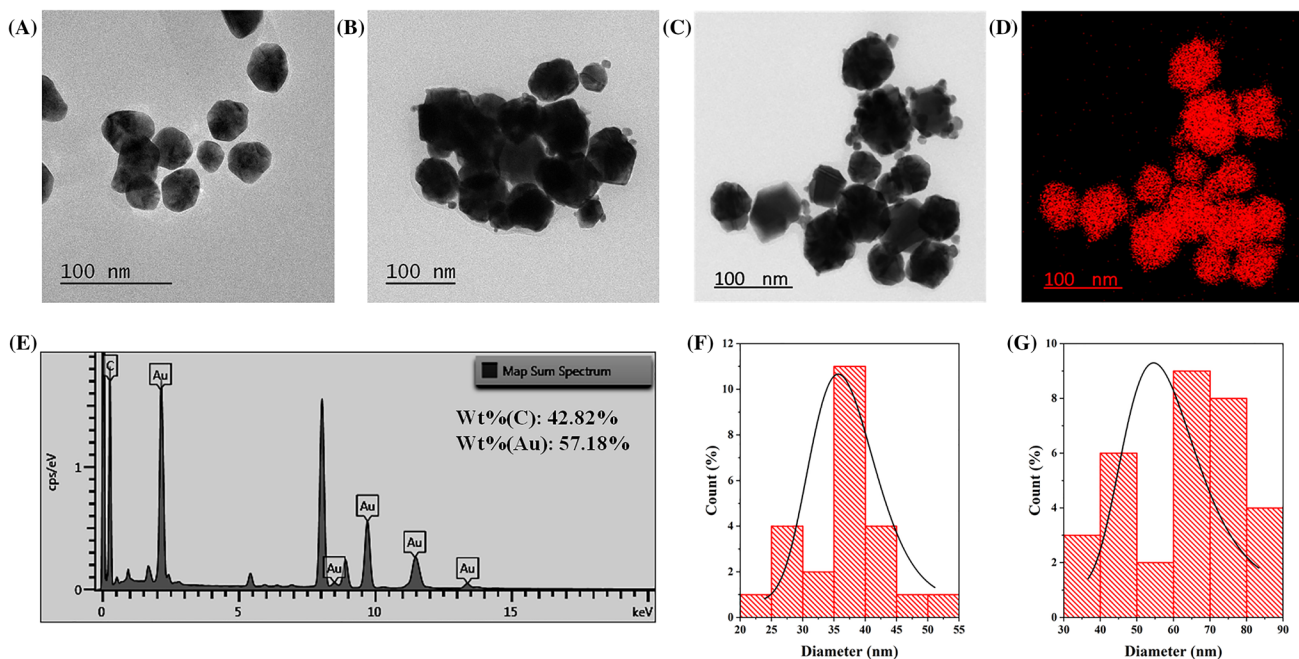


**Fig. 6** Field emission transmission electron microscopy (FE-TEM) observation of Tp-AuNPs (A), CST-Tp-AuNPs (B) and Apt-CST-Tp-AuNPs (C) energy-dispersive X-ray spectroscopy (EDS) based map-

ping (D) and chromatograph (E) for Apt-CST-Tp-AuNPs, particle size distribution of Tp-AuNPs (F) and Apt-CST-Tp-AuNPs (G)



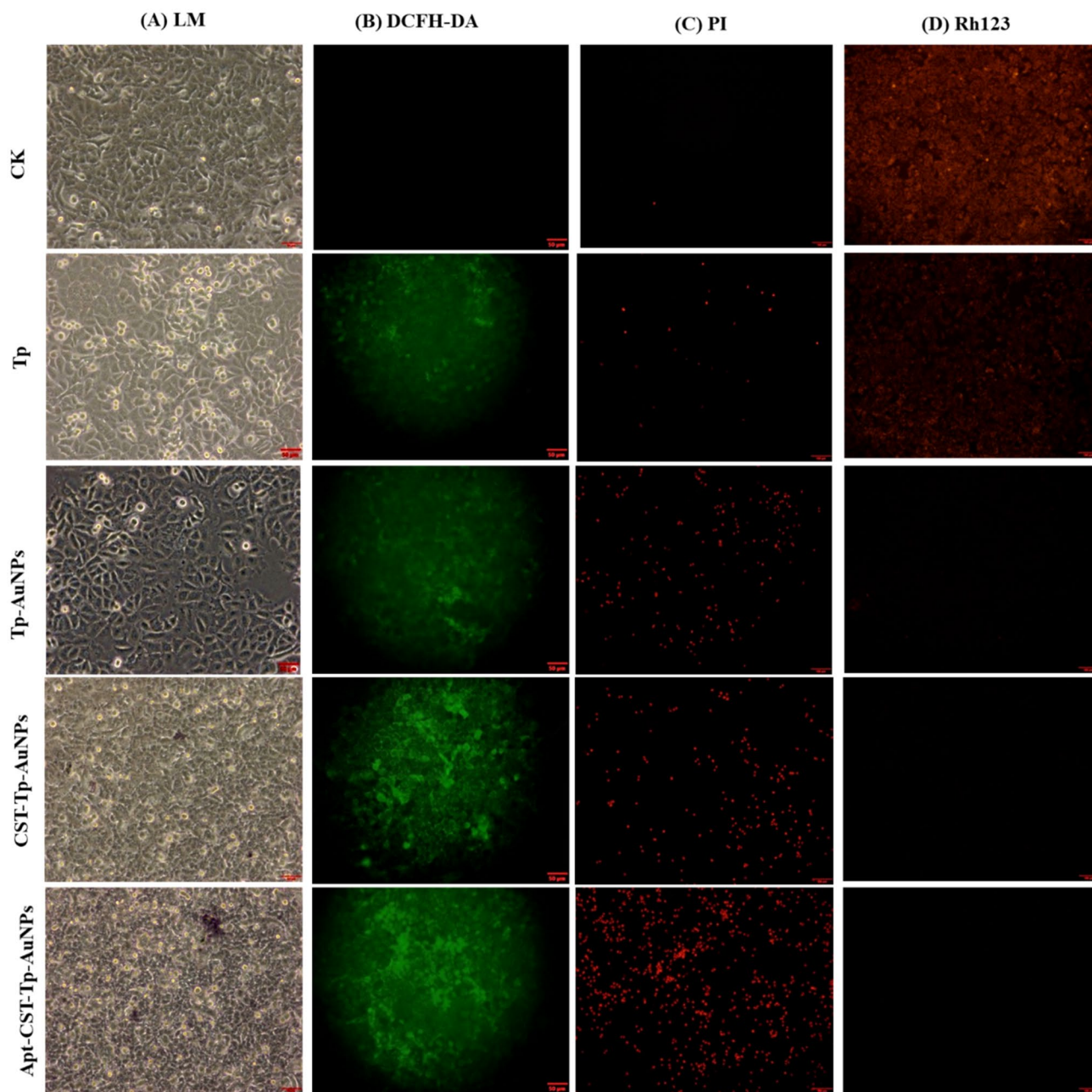


**Fig. 7** Effect of different nanoparticles and mycelial extract treatments in human lung cancer cell line. Light microscope observation of cellular changes (A), DCFH-DA staining for determination of

ROS level (B), the nuclei damage determined by PI strain (C) and the mitochondria membrane loss determined by Rh123 staining (D)

of Tp-AuNPs was found higher in the pH 5.4 than pH7.4 because of the pH-responsive properties of chitosan.

### Cytotoxicity

Cytotoxicity of Tp extract and NPs were tested in the human embryonic kidney cells (HEK293) and human lung cancer cells (A549) by WST assay (SI Fig. 2). All the tested samples were exhibited dose-dependent cytotoxicity in HEK293

or A549. The cell viability of Tp and Tp-AuNPs was significantly lower than the CST-Tp-AuNPs and Apt-CST-Tp-AuNPs in HEK293 (SI Fig. 2A). The Tp and Tp-AuNPs showed higher toxicity in HEK293 cells than the other samples (CST-Tp-AuNPs and Apt-CST-Tp-AuNPs) due to the presence of toxic compounds of fungus [51]. Moreover, the lower nucleolin expression and slower pH reduction in HEK 293 cells prevented the NPs internalization and reduced the pH-sensitive release which leads the less cytotoxicity [12].



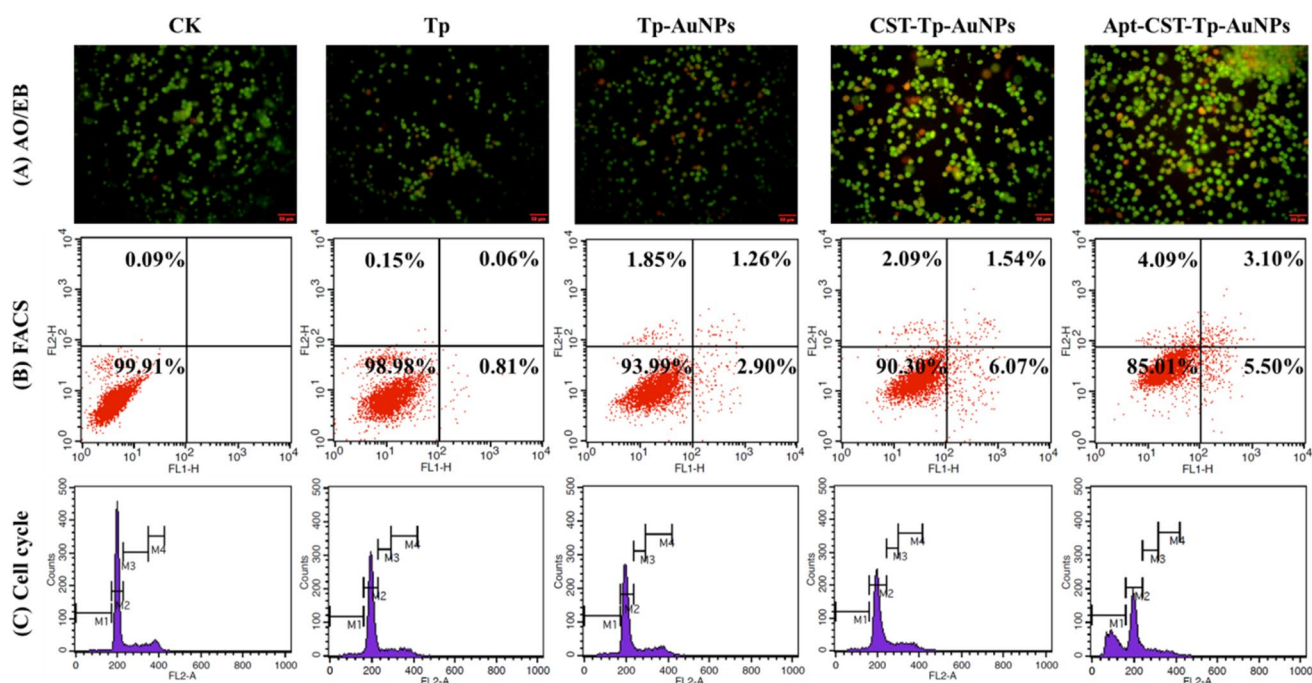


**Fig. 8** Effect of different nanoparticles and mycelial extract on A549 cells. Analysis of apoptosis stages by AO/EB fluorescent staining analysis (A), Annexin v FITC mediated FACS apoptosis analysis (B) and cell cycle analysis (C)

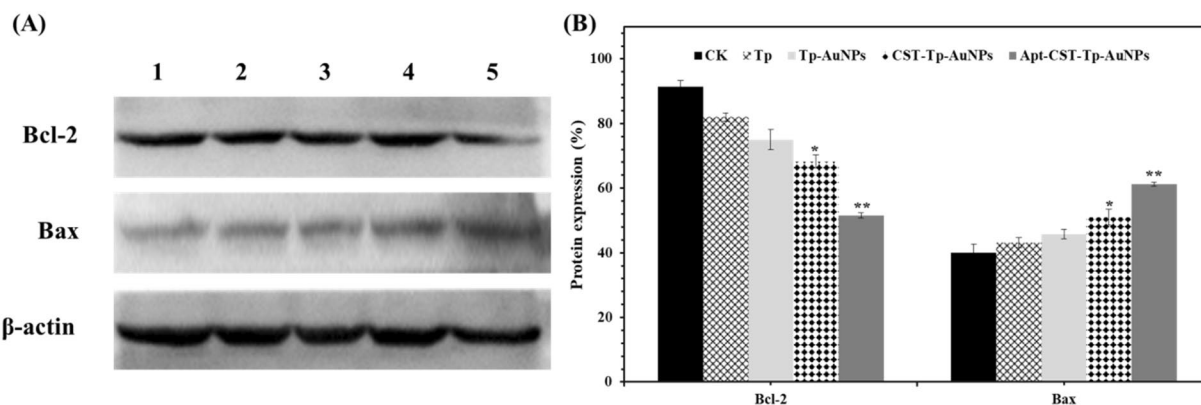


**Fig. 9** The western blotting analysis of apoptosis-related protein expression (Bcl-2 and Bax) (A) and quantification of protein expression (B) in A549 cells treated with different nanoparticles and mycelial extract. 1-CK, 2-Tp, 3-Tp-AuNPs, 4-CST-Tp-AuNPs, 5-Apt-CST-Tp-AuNPs

The acidic pH and higher nucleolin expression in A549 cells enabled the higher internalization and release CST-Tp-AuNPs and Apt-CST-Tp-AuNPs in cells which lead to more effective cytotoxicity in A549 cells compared to Tp and Tp-AuNPs (SI Fig. 2B). The Apt-CST-Tp-AuNPs were not cytotoxicity to HEK293 cells while induced 60% of cell death in A549. Among the samples, the Apt-CST-Tp-AuNPs showed the highest antitumor activity due to nucleolin receptor-targeted and pH-responsive release [52].

### Analysis of apoptosis by fluorescence staining and flow cytometry

The effect of NPs and Tp extract treatment in A549 cells was determined through various fluorescence staining assays (Fig. 7 and SI Fig. 3). The DCFH-DA, PI, and Rh123 were used to determined ROS generation, nucleus damage, and mitochondria membrane loss, respectively [53, 54]. The ROS generation showed the highest intensity from the cells

treated by Apt-CST-Tp-AuNPs (Fig. 7B and SI Fig. 3). Similarly, most of the cell nucleus damage and mitochondria membrane loss occurred in the cells treated by the Apt-CST-Tp-AuNPs (Fig. 7C, D, and SI Fig. 3). Further, the effect of these sample treatments on cell death stages was determined by AO/EB staining, flow cytometry, and cell cycle (Fig. 8). Dual AO/EB staining shows the living cells in translucent green, early apoptotic cells in yellow-green, late apoptotic cells appear in orange or red, and necrotic cells in red color [55]. The AO/EB results indicated that Apt-CST-Tp-AuNPs significantly induce necrotic to A549 cells as demonstrated by the cells stained with orange and red color (Fig. 8A). The FITC annexin V and PI staining results revealed that Apt-CST-Tp-AuNPs induced ~8.60% cell death in A549 cells whereas the Tp-AuNPs and CST-Tp-AuNPs exhibited ~4.16% and 7.61% of cell death in A549 cells (Fig. 8B). Moreover, the cell cycle assay demonstrated that the Apt-CST-Tp-AuNPs induced the M1 phase cell arrest mediated apoptosis (Fig. 8C). Several cellular intrinsic apoptotic pathway-related proteins such as the caspases-3, caspases-6, poly (ADP-ribose) polymerase-1 (PARP-1), Bcl-2, and Bax are known to involve in cell apoptosis [56]. In the present work, the pro-apoptosis (Bax) and anti-apoptosis-related protein (Bcl-2) expressions were analyzed by western blotting. The results revealed that the treatment of Apt-CST-Tp-AuNPs inhibited the expression of Bcl-2 while promoted the Bax to trigger apoptosis (Fig. 9A, B). The sample treatment would cause DNA damage which transfers the signal to the Bcl-2 protein that results in the Bcl-2 and Bax. The Bax induced mitochondrial outer membrane permeabilization, which signals to CytC or Apaf-1 cause Apoptosome [57].

## Conclusion

This work synthesized the myogenic Tp-AuNPs and promoted its cytotoxicity in cancer cells through encapsulation of chitosan and conjugation of the aptamer. The characterization results revealed that the size and shape of the Tp-AuNPs were significantly influenced by chitosan encapsulation. The Apt-CST-Tp-AuNPs were found to be hexagonal with a positive charge while the Tp-AuNPs were spherical with a negative zeta charge. The cytotoxicity of Tp-AuNPs was higher in HEK293 cells compared to Apt-CST-Tp-AuNPs. But Apt-CST-Tp-AuNPs showed the higher cytotoxicity to A549 cells because of aptamer functionalization and acidic pH of cancer cells. Moreover, the various cell cytotoxicity assay evidenced that the Apt-CST-Tp-AuNPs trigger higher cytotoxicity in A549 cells through regulating the ROS generation and apoptosis-related protein expression. Overall, this work concluded that Apt-CST-Tp-AuNPs are deserved for further animal studies to elucidate the molecular mechanism.

**Supplementary Information** The online version contains supplementary material available at <https://doi.org/10.1007/s40097-021-00437-2>.

**Acknowledgements** This work was supported by Brain Pool Program through the National Research Foundation of Korea (NRF) funded by the Ministry of Science, ICT and Future Planning (2017H1D3A1A01052610), National Research Foundation of Korea (2019R1A1055452).

## Declarations

**Conflict of interest** The authors declare that they have no conflict of interest.

## References

1. Siegel, R.L., Miller, K.D., Jemal, A.: Cancer statistics, 2019. *CA A Cancer J. Clin.* **69**(1), 7–34 (2019)
2. Mahalingaiah, P.K., Ciurlionis, R., Durbin, K.R., Yeager, R.L., Philip, B.K., Bawa, B., Mantena, S.R., Enright, B.P., Liguori, M.J., Vleet, T.R.V.: Potential mechanisms of target-independent uptake and toxicity of antibody-drug conjugates. *Pharmacol. Ther.* **200**, 110–125 (2019)
3. Moosavian, S.A., Sahebkar, A.: Aptamer-functionalized liposomes for targeted cancer therapy. *Cancer Lett.* **448**, 144–154 (2019)
4. Xu, L., He, X.Y., Liu, B.Y., Xu, C., Ai, S.L., Zhuo, R.X., Cheng, S.X.: Aptamer-functionalized albumin-based nanoparticles for targeted drug delivery. *Colloid Surf. B-Biointerfaces.* **171**, 24–30 (2018)
5. Yadav, A., Kon, K., Kratosova, G., Duran, N., Ingle, A.P., Rai, M.: Fungi as an efficient mycosystem for the synthesis of metal nanoparticles: progress and key aspects of research. *Biotechnol. Lett.* **37**(11), 2099–2120 (2015)
6. Huang, X., El-Sayed, I.H., Qian, W., El-Sayed, M.A.: Cancer cell imaging and photothermal therapy in the near-infrared region by using gold nanorods. *J. Am. Chem. Soc.* **128**(6), 2115–2120 (2006)
7. Huff, T.B., Tong, L., Zhao, Y., Hansen, M.N., Cheng, J.X., Wei, A.: Hyperthermic effects of gold nanorods on tumor cells. *Nanomedicine* **2**(1), 125–132 (2007)
8. Arokiyaraj, S., Saravanan, M., Badathala, V.: Green synthesis of Silver nanoparticles using aqueous extract of *Taraxacum officinale* and its antimicrobial activity. *South Indian J. Biol. Sci.* **2**, 115–118 (2015)
9. Singh, D.K., Kumar, J., Sharma, V.K., Verma, S.K., Singh, A., Kumari, P., Kharwar, R.N.: Mycosynthesis of bactericidal silver and polymorphic gold nanoparticles: physicochemical variation effects and mechanism. *Nanomedicine* **13**(2), 191–207 (2017)
10. Sathiyaseelan, A., Saravanakumar, K., Mariadoss, A.V.A., Wang, M.H.: pH-controlled nucleolin targeted release of dual drug from chitosan-gold based aptamer functionalized nano drug delivery system for improved glioblastoma treatment. *Carbohydr. Polym.* **262**, 117907 (2021)
11. Saravanakumar, K., Sathiyaseelan, A., Mariadoss, A.V.A., Hu, X., Venkatachalam, K., Wang, M.H.: Nucleolin targeted delivery of aptamer tagged *Trichoderma derived* crude protein coated gold nanoparticles for improved cytotoxicity in cancer cells. *Process Biochem.* **102**, 325–332 (2021)
12. Saravanakumar, K., Sathiyaseelan, A., Mariadoss, A.V.A., Jeevithan, E., Hu, X., Shin, S., Wang, M.H.: Dual stimuli-responsive release of aptamer AS1411 decorated erlotinib loaded chitosan



- nanoparticles for non-small-cell lung carcinoma therapy. *Carbohydr. Polym.* **245**, 116407 (2020)
13. Khiralla, A., Spina, R., Yagi, S., Mohamed, L., Laurain, M.D.: Endophytic fungi: occurrence, classification, function and natural products. *Pub. Univ. Lorraine.* 1–19 (2016)
  14. Shankar, S.S., Ahmad, A., Pasricha, R., Sastry, M.: Bioreduction of chloroaurate ions by geranium leaves and its endophytic fungus yields gold nanoparticles of different shapes. *J. Mater. Chem.* **13**(7), 1822–1826 (2003)
  15. Musarrat, J., Dwivedi, S., Singh, B.R., Al-Khedhairi, A.A., Azam, A., Naqvi, A.: Production of antimicrobial silver nanoparticles in water extracts of the fungus *Amylomyces rouxii* strain KSU-09. *Bioresour. Technol.* **101**(22), 8772–8776 (2010)
  16. Verma, V.C., Singh, S.K., Solanki, R., Prakash, S.: Biofabrication of anisotropic gold nanotriangles using extract of endophytic *Aspergillus clavatus* as a dual functional reductant and stabilizer. *Nanoscale Res. Lett.* **6**(1), 16 (2011)
  17. Rehman, F., Deshmukh, S., Ingle, A., Gade, A., Rai, M.: Silver nanoparticles: novel antimicrobial agent synthesized from an endophytic fungus *Pestalotia* sp. isolated from leaves of *Syzygium cumini* (L). *Nano Biomed. Eng.* **3**, 174–178 (2011)
  18. Kumari, M., Taritla, S., Sharma, A., Jayabaskaran, C.: Antiproliferative and antioxidative bioactive compounds in extracts of marine-derived endophytic fungus *Talaromyces purpureogenus*. *Front. Microbiol.* (2018). <https://doi.org/10.3389/fmicb.2018.01777>
  19. Pandit, S.G., Mekala, R.K.P., Puttananjiah, M.H., Dhale, M.A.: *Cicer arietinum* (Bengal gram) husk as alternative for *Talaromyces purpureogenus* CFRM02 pigment production: Bioactivities and identification. *LWT.* **116**, 108499 (2019)
  20. Pandit, S.G., Puttananjiah, M.H., Harohally, N.V., Dhale, M.A.: Functional attributes of a new molecule-2-hydroxymethyl-benzoic acid 2'-hydroxy-tetradecyl ester isolated from *Talaromyces purpureogenus* CFRM02. *Food Chem.* **255**, 89–96 (2018)
  21. Bhatnagar, S., Kobori, T., Ganesh, D., Ogawa, K., Aoyagi, H.J.N.: Biosynthesis of silver nanoparticles mediated by extracellular pigment from *Talaromyces purpureogenus* and their biomedical applications. *Nanomaterials* **9**(7), 1042 (2019)
  22. Hu, X., Saravanakumar, K., Jin, T., Wang, M.H.: Mycosynthesis, characterization, anticancer and antibacterial activity of silver nanoparticles from endophytic fungus *Talaromyces purpureogenus*. *Int J Nanomedicine.* **14**, 3427–3438 (2019)
  23. Azuma, K., Izumi, R., Osaki, T., Ifuku, S., Morimoto, M., Saimoto, H., Saburo, M., Okamoto, Y.: Chitin, chitosan, and its derivatives for wound healing: old and new materials. *J. Func. Biomater.* **6**(1), 104–142 (2015)
  24. Abdelhamid, H.N., El-Bery, H.M., Metwally, A.A., Elshazly, M., Hathout, R.M.: Synthesis of CdS-modified chitosan quantum dots for the drug delivery of Sesamol. *Carbohydr. Polym.* **214**, 90–99 (2019)
  25. Dowaidar, M., Nasser, A.H., Hällbrink, M., Langel, Ü., Zou, X.: Chitosan enhances gene delivery of oligonucleotide complexes with magnetic nanoparticles–cell-penetrating peptide. *J. Biomater. Appl.* **33**(3), 392–401 (2018)
  26. Wang, F., Zhang, Q., Li, X., Huang, K., Shao, W., Yao, D., Huang, C.: Redox-responsive blend hydrogel films based on carboxymethyl cellulose/chitosan microspheres as dual delivery carrier. *Int. J. Biol. Macromol.* **134**, 413–421 (2019)
  27. Fathi, M., Majidi, S., Zangabad, P.S., Barar, J., Erfan-Niya, H., Omidi, Y.: Chitosan-based multifunctional nanomedicines and theranostics for targeted therapy of cancer. *Med. Res. Rev.* **38**(6), 2110–2136 (2018)
  28. Abdelhamid, H.N., Dowaidar, M., Langel, Ü.: Carbonized chitosan encapsulated hierarchical porous zeolitic imidazolate frameworks nanoparticles for gene delivery. *Microporous Mesoporous Mat.* **302**, 110200 (2020)
  29. Saravanakumar, K., Wang, M.H.: *Trichoderma* based synthesis of anti-pathogenic silver nanoparticles and their characterization, antioxidant and cytotoxicity properties. *Microb. Pathog.* **114**, 269–273 (2018)
  30. Saravanakumar, K., Jeevithan, E., Chelliah, R., Kathiresan, K., Wen, H.W., Oh, D.H., Wang, M.H.: Zinc-chitosan nanoparticles induced apoptosis in human acute T-lymphocyte leukemia through activation of tumor necrosis factor receptor CD95 and apoptosis-related genes. *Int. J. Biol. Macromol.* **119**, 1144–1153 (2018)
  31. Saravanakumar, K., Hu, X., Shanmugam, S., Chelliah, R., Sekar, P., Oh, D.H., Vijayakumar, S., Kathiresan, K., Wang, M.H.: Enhanced cancer therapy with pH-dependent and aptamer functionalized doxorubicin loaded polymeric (poly D, L-lactic-co-glycolic acid) nanoparticles. *Arch. Biochem. Biophys.* **671**, 143–151 (2019)
  32. Saravanakumar, K., Vivek, R., Sithranga, B.N., Yaqian, L., Kathiresan, K., Chen, J.: Anticancer potential of bioactive 16-methylheptadecanoic acid methyl ester derived from marine *Trichoderma*. *J. Appl. Biomed.* **13**(3), 199–212 (2015)
  33. Liu, N., Zhang, T., Cao, B.R., Luan, F.Y., Liu, R.X., Yin, H.R., Wang, W.B.: Icarin possesses chondroprotective efficacy in a rat model of dexamethasone-induced cartilage injury through the activation of miR-206 targeting of cathepsin K. *Int. J. Mol. Med.* **41**(2), 1039–1047 (2018)
  34. Amendola, V., Meneghetti, M.: Size evaluation of gold nanoparticles by UV–VIS spectroscopy. *J. Phys. Chem. C.* **113**(11), 4277–4285 (2009)
  35. Clarence, P., Luvankar, B., Sales, J., Khusro, A., Agastian, P., Tack, J.C., Khulaifi, M.M.A., Shwaiman, H.A.A., Elgorban, A.M., Syed, A., Kim, H.J.: Green synthesis and characterization of gold nanoparticles using endophytic fungi *Fusarium solani* and its in-vitro anticancer and biomedical applications. *Saudi J. Biol. Sci.* **27**(2), 706–712 (2020)
  36. Manjunath, H.M., Joshi, C.G., Raju, N.G.: Biofabrication of gold nanoparticles using marine endophytic fungus–*Penicillium citrinum*. *IET Nanobiotechnol.* **11**(1), 40–44 (2017)
  37. Huang, H., Yang, X.: Synthesis of chitosan-stabilized gold nanoparticles in the absence/presence of tripolyphosphate. *Biomacromol* **5**(6), 2340–2346 (2004)
  38. Hamdy, M.E., Del, C.M., Hussein, H.A., Salah, T.A., El-Deeb, A.H., Emara, M.M., Pezzoni, G., Compagnone, D.: Development of gold nanoparticles biosensor for ultrasensitive diagnosis of foot and mouth disease virus. *J. Nanobiotechnol.* **16**(1), 48 (2018)
  39. Suvarna, S., Espinasse, B., Qi, R., Lubica, R., Poncz, M., Cines, D.B., Wiesner, M.R., Arepally, G.M.: Determinants of PF4/heparin immunogenicity. *Blood* **110**(13), 4253–4260 (2007)
  40. Hemashekhar, B., Chandrappa, C.P., Govindappa, M., Chandrashekar, N.: Endophytic fungus *Alternaria* spp isolated from *Rauvolfia tetraphylla* root arbitrate synthesis of gold nanoparticles and evaluation of their antibacterial, antioxidant and antimitotic activities. *Adv. Nat. Sci. Nanosci. Nanotechnol.* **10**(3), 035010 (2019)
  41. Uzma, M., Raghavendra, V., Girish, S.: Biogenesis of gold nanoparticles, role of fungal endophytes and evaluation of anticancer activity—a review. *Eur. J. Biomed. Pharm. Sci.* **5**, 319–329 (2018)
  42. Parmar, S., Sharma, V.K.: 13-Endophytic fungi mediated biofabrication of nanoparticles and their potential applications. In: Kumar, A., Singh, V.K. (eds.) *Microbial endophytes*, pp. 325–341. Woodhead Publishing, Cambridge (2020)



43. Zambito, Y.: Nanoparticles based on chitosan derivatives. In: *Advances in Biomaterials Science and Biomedical Applications*, pp. 243–63 (2013)
44. Chowdhury, P., Roy, B., Mukherjee, N., Mukherjee, S., Joardar, N., Mondal, M.K., Roy, D., Babu, S.P.S.: Chitosan biopolymer functionalized gold nanoparticles with controlled cytotoxicity and improved antifilarial efficacy. *Adv. Compos. Hybrid Mater.* **1**(3), 577–590 (2018)
45. Sneha, K., Esterle, A., Sharma, N., Sahi, S.: Yucca-derived synthesis of gold nanomaterial and their catalytic potential. *Nanoscale Res. Lett.* **9**, 627 (2014)
46. Brady, J.B., Boardman, S.J.: Introducing mineralogy students to x-ray diffraction through optical diffraction experiments using lasers. *J. Geol. Educ.* **43**(5), 471–476 (1995)
47. Quideau, S., Deffieux, D., Douat, C.C., Pouységu, L.: Plant polyphenols: chemical properties, biological activities, and synthesis. *Angew. Chem. Int. Ed.* **50**(3), 586–621 (2011)
48. Chai, Y.J., Cui, C.B., Li, C.W., Wu, C.J., Tian, C.K., Hua, W.: Activation of the dormant secondary metabolite production by introducing gentamicin-resistance in a marine-derived *Penicillium purpurogenum* G59. *Mar Drugs.* **10**(3), 559–582 (2012)
49. Sathiyaseelan, A., Shajahan, A., Kalaichelvan, P.T., Kaviyarsan, V.: Fungal chitosan based nanocomposites sponges—an alternative medicine for wound dressing. *Int. J. Biol. Macromol.* **104**, 1905–1915 (2017)
50. Choi, S.J., Ban, C.: Crystal structure of a DNA aptamer bound to PvLDH elucidates novel single-stranded DNA structural elements for folding and recognition. *Sci. Rep.* **6**(1), 34998 (2016)
51. Houbraken, J., de Vries, R.P., Samson, R.A.: Chapter four-modern taxonomy of biotechnologically important *Aspergillus* and *Penicillium* species. In: Sariaslani, S., Gadd, G.M. (eds.) *Adv. Appl. Microbiol.*, pp. 199–249. Academic Press, Cambridge (2014)
52. Wike, H.J.L., Haveman, J., Reinhold, H.S.: The relevance of tumour pH to the treatment of malignant disease. *Radiother. Oncol.* **2**(4), 343–366 (1984)
53. Saravanakumar, K., Mandava, S., Chellia, R., Jeevithan, E., Babu, Y.R.S., Mandava, D., Wu, W.H., Lee, J., Oh, D.H., Kathiresan, K., Wang, M.H.: Novel metabolites from *Trichoderma atroviride* against human prostate cancer cells and their inhibitory effect on *Helicobacter pylori* and *Shigella toxin* producing *Escherichia coli*. *Microb. Pathog.* **126**, 19–26 (2019)
54. Saravanakumar, K., Shanmugam, S., Varukattu, N.B., MubarakAli, D., Kathiresan, K., Wang, M.H.: Biosynthesis and characterization of copper oxide nanoparticles from indigenous fungi and its effect of photothermolysis on human lung carcinoma. *J. Photochem. Photobiol. B-Biol.* **190**, 103–109 (2019)
55. Narayani, S.S., Saravanan, S., Ravindran, J., Ramasamy, M.S., Chitra, J.: In vitro anticancer activity of fucoidan extracted from *Sargassum cinereum* against Caco-2 cells. *Int. J. Biol. Macromol.* **138**, 618–628 (2019)
56. Chandra, D., Tang, D.G.: Detection of apoptosis in cell-free systems. *Methods Mol. Biol.* **559**, 65–75 (2009)
57. Messner, B., Frotschnig, S., Steinacher, N.A., Winter, B., Eichmair, E., Gebetsberger, J., Schwaiger, S., Ploner, C., Laufer, G., Bernhard, D.: Apoptosis and necrosis: two different outcomes of cigarette smoke condensate-induced endothelial cell death. *Cell Death Dis.* **3**(11), e424 (2012)

**Publisher's Note** Springer Nature remains neutral with regard to jurisdictional claims in published maps and institutional affiliations.

